Journal of Manufacturing Systems 50 (2019) 69–80

Contents lists available at ScienceDirect

Journal of Manufacturing Systems

journal homepage: www.elsevier.com/locate/jmansys

Five-axis additive manufacturing of freeform models through buildup of transition layers

Mohammed A. Isa, Ismail Lazoglu*

Koc University, Manufacturing and Automation Research Center, Mechanical Engineering Department, Rumelifeneri Yolu, Sariyer, Istanbul, 34450, Turkey

ARTICLE INFO

Keywords:
Staircase effect
Stairstep effect
Additive manufacturing
5-axis additive manufacturing
Path planning

ABSTRACT

Acclaimed for enabling the fabrication of complex parts, additive manufacturing is confined to established processing and planning methods that contribute impediments to its industrial adoption. The requirement of support structures and poor quality of produced surfaces are some of these impediments. Extension of the manufacturing method to accommodate variable tool orientation can introduce new approaches in process planning that can resolve these obstacles. Therefore, a new 5-axis 3D printer is designed, built and programmed to facilitate implementation of novel 3D curve paths. Common layering methods in additive manufacturing are centered around the idea of intersection of a CAD model with parallel planes or offset surfaces without regards to the form of the part. The use of these inflexible layering patterns leads to staircase effect on the surfaces, inefficient toolpaths and low load-bearing capacity. This article suggests and develops new 5-axis path planning model that takes into account the surface profiles of the freeform part. Path and tool orientation conditions are reexamined to propose planning schemes that prevent staircase effects on shell and solid components. To accomplish this, the material is deposited on successive transition surfaces whose intra-layer thickness varies to allow changes in the form of the surfaces.

1. Introduction

Additive manufacturing (AM) or three-dimensional (3D) printing has grown continuously since its inception in the 1980s. Parts are manufactured by a successive layer-on-layer based material deposition along paths that are generated directly from a computer-aided design (CAD) model. Manufacturing of various materials ranging from flexible polymers to strong metals can now be realized additively. AM applications has also proliferated to a wide scope of research stretching from nano-scale bio-fabrication to large architectural constructions [1]. The most ubiquitous AM method is the fused deposition modeling® (FDM) or fused filament fabrication (FFF), which relies on the malleability of thermoplastics at low temperature for deposition of molten material to form the solid part. FDM is significantly cheaper than other AM methods, such as selective laser sintering/melting (SLS/SLM) used for metals, however, it is still predominantly confined to the fabrication of prototyping components [2]. The lack of reliability and consistency in material properties and dimensional accuracy hinders the adoption of AM in the rigorous industrial production environment [3]. For AM to satisfy more demanding applications, it becomes necessary to address the hurdles holding back its promise of revolution in manufacturing.

To open up new avenues of research, classic uniaxial AM design can be expanded to multi-axis AM (MAAM) concept. In addition to the common three-axis relative motion between tool and workpiece, multi-axis systems have one or more additional direction(s) of movement that allows variable tool orientations. Multi-axis manufacturing is not a new notion seeing that it is has gained ground in machining field with an extensive research background and advanced application in production of complex parts. On the contrary, when it comes to AM, the available research, hardware and software in MAAM is inadequate and requires an overhaul of the present facilities [4].

Mechanical strength and geometric accuracy of produced parts are major concerns in AM. The surface quality of additively manufactured parts is affected by stairstep (or staircase) phenomenon which leaves ridges in the size of layer thickness on surfaces that are supposed to be smooth. In addition to deviation in shape, staircase effect also necessitates postprocessing operations like polishing [5]. Surface quality of top and side profiles in FDM have been analyzed by Jin et al. [6], where mathematical models of surface deviations are explored.

By the addition of z-axis to common 2D layer path of three-axis 3D printers, Chakraborty et al [7] introduce the idea of curved layer fused deposition (CLFD) modeling. This method uses a curved layer where deposition path normal vectors deviate only slightly away from the vertical. Llewellyn-Jones [8], Allen and Trask [9] demonstrated CLFD

* Corresponding author.
E-mail address: ilazoglu@ku.edu.tr (I. Lazoglu).

https://doi.org/10.1016/j.jmsy.2018.12.002
Received 26 June 2018; Received in revised form 22 October 2018; Accepted 3 December 2018
Available online 10 December 2018

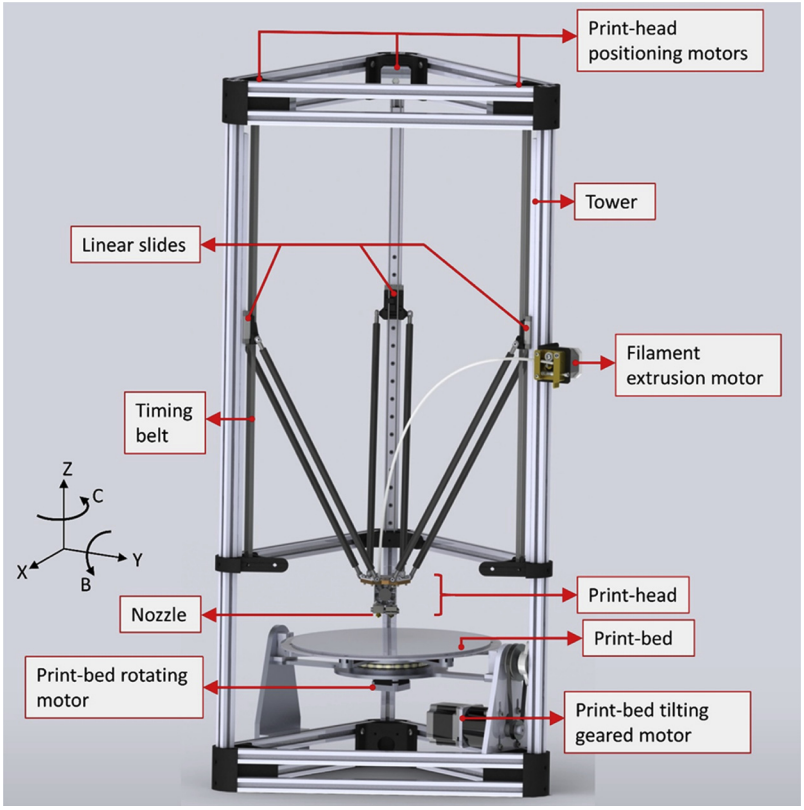

Fig. 1. 5-axis 3D printer design showing actuators and mechanical components of the system.

application in manufacturing of skin surfaces in composite and multi-material structures to reduce stairstep effects. Recently, in the modeling and process planning of CLFD [10], the demand for a universal slicing method for arbitrary model is emphasized. The disadvantages of using three-axis 3D printers for curved layers includes limited surface geometry and the possibility of shearing and scraping during deposition. Since the CLFD in literature uses uniaxial deposition, issues like requirement of support structure and staircase effects (especially on side surfaces) are still predominant. As a result, an ideal curved layer 3D printing is envisioned using 5-axis gantry [7,10]. Pertaining to mechanical strength, It has been shown that 3D printed parts are anisotropic and have the highest strength along the deposition raster's direction [11]. The incorporation of fiber reinforcement in this direction can further increase this strength manifold [2]. Singamneni et al. [12] showed that using curved layer path can improve the load a part can withstand. In light of these prospects, it becomes necessary to explore new paradigms in additive fabrication of parts where tailoring 3D raster direction is feasible.

An important aspect of most manufacturing methods is path planning. For subtractive and additive manufacturing alike, the toolpath determines the quality of the part produced. Considering the nature of machining, parts can be machined starting from any region and orientation as long as it leads to the desired geometry. Hence, for the many machining operations, various toolpath have been studied with objectives like optimization of production time [13] and geometric accuracy [14]. On the other hand, AM is constrained to begin from a given build layer and configuration. Perhaps, this is the reason why AM has less diverse toolpath and its multi-axis strategies has not been equally studied exhaustively. There are several commercial multi-axis CAM packages for machining, but there is lack of such for AM [15]. Using conventional slicers, it is possible to sequentially 3D print parts in discrete build orientations. To eliminate the need for supports, a digital model, in STL (StereoLithography) file, can be partitioned algorithmically and fabricated at different build orientation using a multi-axis system [16]. The use of these planar slicers narrows the applicability of MAAM by restricting depositions to planar paths. For instance, it will not be possible to carry out 5-Axis AM, where 3D printing paths of 3D curves demand instantaneous mingling of the all the axes of motion. Grutle [17] designed a 5-axis 3D printer to show the possibility of fabrication with better surface quality and without requirement of supports. These improvements are demonstrated on simple parts and the lack of a 5-axis slicer for general 3D printing is mentioned as a main issue. In another work [18], the build table is attached to a robotic arm to accomplish multi-axis AM using commercial machining CAM software for path planning. Most recently, Shen et al. [15] proposed slicing methods of 5-axis AM by intersection of offset surfaces for non-planar sculpture-printing and tangential tool direction for shell parts. Concerning the amount of material deposited, development of AM process where the shape of layers deforms—contrary to the use of parallel planes or offset surfaces—will require non-uniform material buildup and variable material extrusion rate within each layer. Indeed, the prospects of studying new AM layering combined with the new realm of possibilities facilitated by MAAM, commonly affirmed in the available studies, can extend AM development and application. With a complete multi-axis AM process for freeform parts, integration to combined additive and subtractive scheme can be a promising endeavor [19].

In this article, a new approach in model representation, geometric computation and path planning is explored to address some of the setbacks of AM. Initially, Section 2 presents design alternatives of a 5-axis 3D printer, introduces the selected mechanical design, and outlines features of its control system. Next, Section 3 proposes methods of path planning for arbitrary shell and solid models. Considering build orientations requirements and shape of model's geometry, strategies in construction of buildup layers and path are explored. Finally, Section 4 covers the evaluation of build angles and analysis of kinematic error.

2. Design of the 5-axis 3D printer

A 5-axis 3D printer is designed and reconstructed by extension of a modified open-source design. The RepRap project [20] brought 3D printing to the open-source community in 2011 and has been expanded to many designs ever since. One of such designs is the delta-type prototype [21], whose variant forms include three pair of moving parallel arms that hold the print-head in place during 3D printing operation. A more popular design is the Cartesian gantry design that is usually composed of drives along the X and Y axes and a moving platform along Z. It is observed that augmentation of additional realm of motion in the delta-type model is less bulky compared with the Cartesian type. Besides, Cartesian design is shown to be slower and less productive [22]. Fig. 1 shows the Delta design with its parallel-arm mechanism that supports and positions the print-head. A slider connected to each pair of arms is positioned vertically by a belt that is attached to the slider in a pulley-belt system, which is solely controlled by a motor above each tower. The positions of the sliders on the three towers dictate the 3D position of the print-head, where the essential process of additive manufacturing takes place. Within the print-head, a thermoplastic filament is injected, heated and deposited through the nozzle. The filament is fed with the aid of an additional motor and the heating is carried out by a resistive cartridge heater where temperature is regulated by a thermistor.

2.1. Mechanical design of the 3D printer

Delta type 3D printers, along with other common 3D printing designs, are capable of manipulating 3D printing nozzle only in the translational axes X, Y and Z. The build direction which is along the nozzle deposition direction is usually fixed in the Z direction for such 3-axis systems. Confined by the constant build direction, the scope of AM is diminished to the incorporation of only Z planar deposition paths. In this paper, a 3D printer inspired by the described delta-type concept is designed with two additional degrees of freedom resulting from the rotation and tilting of the print-bed, as shown in Fig. 1. Optionally, the added rotational motions can be given to the print-head instead of the print platform. Decision on adding motion to the platform rather than the print-head is based on both simplicity [22] and concern of added load on the parallel arms. Besides, keeping the nozzle aligned with gravitational acceleration assists in material deposition. The print-bed rotation about C axis is controlled by the motor attached to the base of the bed platform. The second rotation, about B axis, permits tilting of the whole print-bed via a belt that is linked with a planetary geared motor. The designed printer has a cylindrical working space of about 210 mm diameter and 200 mm height.

Expansion of 3D printing tool movement with respect to the workpiece beyond 3-axis unleashes new possibilities in toolpath design. In literature, 5-axis AM system with two additional rotational have been tested. Yerazunis et al. [23] added an AB type rotary table to a 3D printer where manufacturing of hemispherical pressure cap is studied. Shen et al. [15] utilized an interference-free nozzle in 5-axis AM to test surface guided offset toolpaths for different modes of 3D printing.

2.2. Controller of the 3D printer

Having designed and assembled the 3D printer, it is necessary to control the motion of the nozzle and print-bed. Just like in computer numerical control (CNC) systems, there is need for a central control unit, where all the actuation and sensory signals are processed. In 3D printing jargon, the control unit is synonymous to a microprocessor board with an installed compatible firmware software. ATmega2560 microprocessor loaded with a designed software based on the open source framework, Marlin firmware [24], is used in this work. Since the original firmware only supports 3-axis 3D printers, new submodules are programmed to extend it to support 5-axis functions. Fig. 2 shows the simplified data flow in the control unit. The commands are classified and added to the command buffer for queuing and redirection to the motion planner. The motion planner mixes the required motion steps of each motor smoothly and the pulse signals are sent to the motor drivers. New G-code commands, G6 and G7, are introduced to handle 2D rotation of the build platform. Only direct positional commands are processed in the control unit. Therefore, the required transformation of 3D printing path is carried out in the post-processing stage because the control unit cannot handle complex calculations with the required speed.

3. Path planning

A vital process in AM, and most of other manufacturing methods, is toolpath planning. At the path planning stage, a set of position coordinates—including orientation information for multi-axis systems—is chosen with respect to the workpiece that is to be manufactured. Regardless of whether or not the part remains stationary during the manufacturing operation, the path generated in the workpiece frame remains equally useful. This is because the path can be transformed to any position the workpiece is moved to. As a result, a complete toolpath can be used in any manufacturing setup such as 3-axis, multi-axis and robotic manufacturing processes. In general, the toolpath is prepared to conform with the nature of the manufacturing method. Extrusion-based additive manufacturing work on the condition that each point on the toolpath must be structurally supported along the deposition direction. Hence, when building a part, choosing a layer path containing points that cannot be supported by preceding layers should be avoided. This is a significant constraint on AM toolpath design that limits how freely lines and curves can be chosen to fill a freeform model. For common 3-axis systems, several toolpath methods have been conventionalized for both machining and AM in the Literature.

Most of path planning in additive manufacturing comes from slicing a workpiece in the format of STL (STereoLithography), a tessellation of a CAD model obtainable in major modeling software packages. The basic slicing relies on finding intersection of tessellation triangles and parallel horizontal planes equally spaced to find the outline of each slice. Due to staircase effect that significantly affects the surface quality, layer and region based adaptive slicing methods are introduced [25]. These methods can only improve the surface quality at the cost of additional deposition layers that increases production time. In fact, the production time increases exponentially as the number of layers increases [5]. In MAAM, planar slicers can be used when the workpiece is partitioned so that separate build directions can be used for each partition to avoid the use of support structures [16]. However, the use of planar slicers in MAAM does not address the problem of stairstep effects.

In addition to producing good surface quality, each point on the path of AM is required to be supported by a solid membrane beneath the point along the build direction. Since the build direction cannot be changed in 3-axis AM, use of support structures may be inevitable [4]. Despite endeavors in CLFD and inclined layer AM [26], 3-axis manipulation of extruder is inadequate in ensuring good surface quality of parts without the use of support structures. For the MAAM in this paper, with the aim of improving surface quality, paths will be constructed without considering the option of using supports. This section covers freeform model representations and the proposed path and build orientation of 5-axis additive manufacturing.

3.1. Freeform solid representation

The two types of commonly used internal solid representation are the Boundary representation (B-rep) and the Constructive Solid Geometry representation (CSG-rep) [27]. For CAD and geometric modeling within engineering applications, B-rep is widely adopted and employed by most modern modeling software packages. Freeform

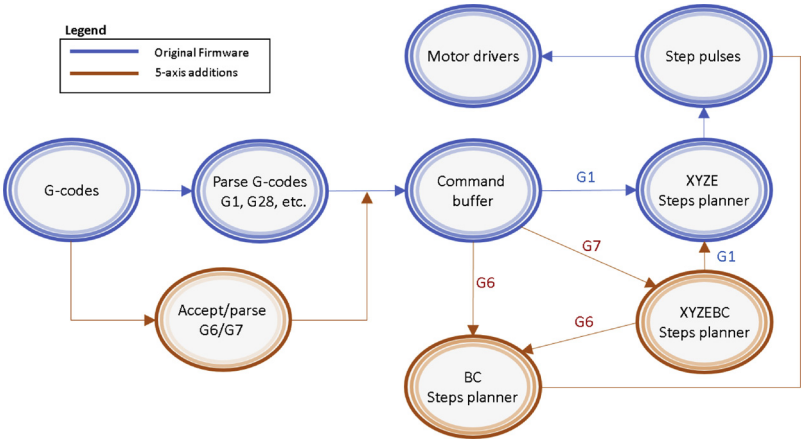

Fig. 2. Simplified process of the control unit (firmware) software showing the modifications to accommodate 5-axis AM.

shapes in this work are represented by B-rep as a collection of trimmed non-uniform rational B-Spline (NURBS) faces, edges and vertices. A NURBS surface $\boldsymbol{S}(u, v)$ is a bivariate vector-valued piecewise rational function [28], which can be evaluated for any parameter values $u\varepsilon[u_0, u_1]$ and $v\varepsilon[v_0, v_1]$. Unlike the popular tessellation based slicers, the direct use of NURBS preserves the surface accuracy of a CAD model [29]. The modeling package Rhinoceros® is used to access shape data from CAD features that is used to plan the multi-axis toolpath. All surface data—like parametric domain, location, derivatives, etc.—are reachable through the scripting environment. To be able to carry out toolpath planning for freeform geometry, a conventional system of organizing the surfaces is adopted.

A plugin script is programmed to process freeform solids in STEP, IGES and Rhino model formats. A CAD model of a freeform part is disintegrated into its component surfaces and edges through the process depicted in Fig. 3. Initially, the extracted surfaces undergo an organizational process of parametric flipping and reversing, which is carried out automatically by the plugin. The requirement for closed surfaces is that each edge of a surface, which is coincident with the bounding isoparametric line, is paired with other edge from another surface. The parametric directions of the surfaces are to fit a specific conventional order shown in Fig. 4. The figure shows the parametric directions of top $\boldsymbol{T}(u, v)$, base $\boldsymbol{B}(u, v)$, and side surfaces of a freeform solid after they are aligned. The parametric directions of the top and base faces are aligned to match each other along the build direction. The side surfaces ($\boldsymbol{S}_1$, $\boldsymbol{S}_2$, $\boldsymbol{S}_3$, ...) are enumerated starting from the parametric origin edge and continuing in counterclockwise directions. The v parameter direction is chosen as upward build direction on the bounding side faces.

3.2. Side surface tangent tool orientation along 3D path

Surface quality of parts manufactured by planar slicing are affected by staircase effect, which becomes more pronounced as shift in the outline of consecutive layers increases. With the introduction of MAAM, it is possible to theoretically eliminate this effect by changing the local

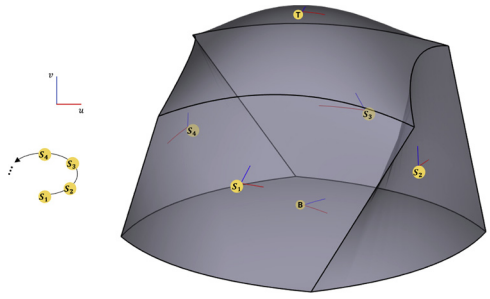

Fig. 4. Alignment and arrangement of surfaces from a freeform model.

nozzle direction [15]. When the build orientation is chosen to remain tangent to the side surfaces, the deviation caused by the staircase effect becomes significantly diminished. Hence, the side surface tangent (SST) tool orientation is adopted as a constraint on the orientation of outline paths of all layers. Since the top surface of a freeform model can also have this effect, the staircase effect is not limited to the side surfaces. This paper also suggests compelling the toolpath at the final layer to remain normal to the top surface. To accomplish this, the intermediate layers used in filling a model to its top surface are constructed as 3D surfaces where the tool direction must remain normal to the surfaces. The described transition surface normal (TSN) tool orientation ensures that the top surface has no stairsteps. The generation of such surfaces and paths challenges present 3D printing layering methods.

Apart from the popular planar slicing methods, an offset method suggested for 3D printing on a non-planar base surface has been studied [15,30]. In this method, by using either mesh or parametric model, a successive offset of nonplanar base surface is intersected with the model to generate layer contours. Despite the added flexibility in layers, the offset method does not address staircase effect on any portion of the manufactured part. Fig. 5 shows three layering methods for a solid model with an exaggerated demonstration of how layers are constructed. The planar slicing method (Fig. 5b) is the most restrictive

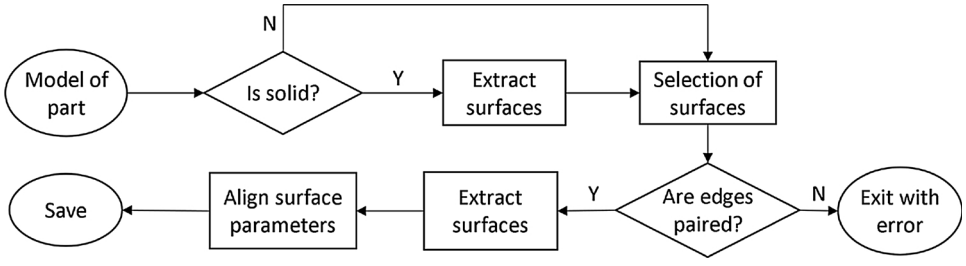

Fig. 3. Procedure of representation of a CAD model as organized connected surfaces.

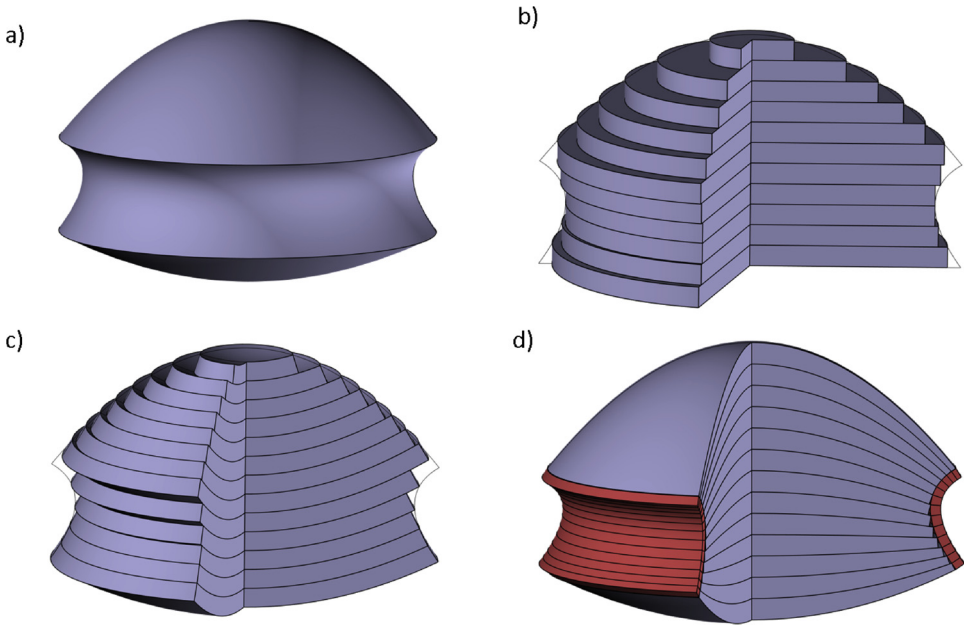

Fig. 5. Stairstep effect of an ideal part in fig. a is demonstrated on b) planar slicer, c) offset surface slicing and d) interior infill and outline (in red) of transition layers (For interpretation of the references to colour in this figure legend, the reader is referred to the web version of this article).

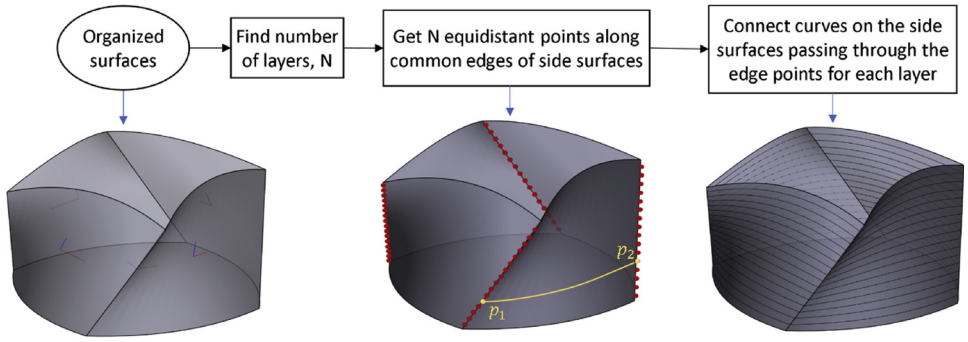

Fig. 6. The algorithm used to generate 3D curves from side surfaces. Connection of edge points $p_1 and\, p_2$ with surface curves is demonstrated.

because it cannot be used for parts that do not have planar base. The offset layering (Fig. 5c) works for nonplanar path, but it only considers the base surface and not the form of other bounding surfaces of the part. Hence, it does not provide solution for staircase effect on the final product. The method suggested in Fig. 5d is based on using a gradual shapeshifting transition layers to fill solid model from the base to top surface. The method also proposes the use of side NURBS surface in constructing the outline portion of each layer (represented in color red). The curves used in generation of the outline path also exhibit the same progressive shape bending to fit the top outline from the base. In this sub-section, generation of paths on side surfaces are discussed for the fabrication of a shell part or the side-exterior portion of a solid model. Together with the strategies developed in this sub-section, Section 3.3 will discuss the transitional layering method of filling a solid model as imagined in Fig. 5d. By comparing how the jagged profiles differ from the desired model in Fig. 5a, it is obvious that the new approach provides the best surface quality among the three methods.

Mapped parametric lines provide curves that initially take the shape of the base and slowly morph to the shape of the top. The form change is possible only if the gaps between consecutive curves varies within a layer. This intra-layer variable thickness can be achieved if the amount of filament extruded at each point reflects this thickness. By conservation of volume, a cylindrical filament, with a diameter D_f deformed into a raster of rectangular cross-section of width w_t and length spanning from (x_i, y_i, z_i) to $(x_{i+1}, y_{i+1}, z_{i+1})$ at a point of local layer thickness of Δl_i, should have filament extrusion length (ΔE_i) given by Eq. 1.

$$\Delta E_i = \frac{4 w_t \Delta l_i \sqrt{(x_{i+1} - x_i)^2 + (y_{i+1} - y_i)^2 + (z_{i+1} - z_i)^2}}{\pi D_f^2} \tag{1}$$

In common FDM printers, the material extrusion rate is known the moment the path positions are found, because the rate of material extrusion is uniformly correlated with the tool velocity. For the shape-changing layers, the rate of material extrusion varies based on the spatial variation in the build of each layer. The length ΔE_i given in Eq. 1 is added to the previous E -motion value in the path and is appended to the g-code sent to the numerical controller. Even though the path points are sampled at a uniform distance within the range 0.4-0.8 mm along the path curve, raster thickness remains uniform throughout the length. The reason for the uniformity is attributed to the linear interpolator in the numerical controller.

For a thin walled freeform part or sides of a filled part, where the side walls are to be fabricated, Fig. 6 shows how the path is constructed. After the surfaces are aligned according to the convention mentioned, the required number of layers is determined. By determining the length of the longest curve from the base to the top edges, using a target maximum layer thickness, the number of layers (N) can be evaluated by dividing the length by the thickness. Next, N points are uniformly distributed along each of the common edges of the surfaces. Curves are

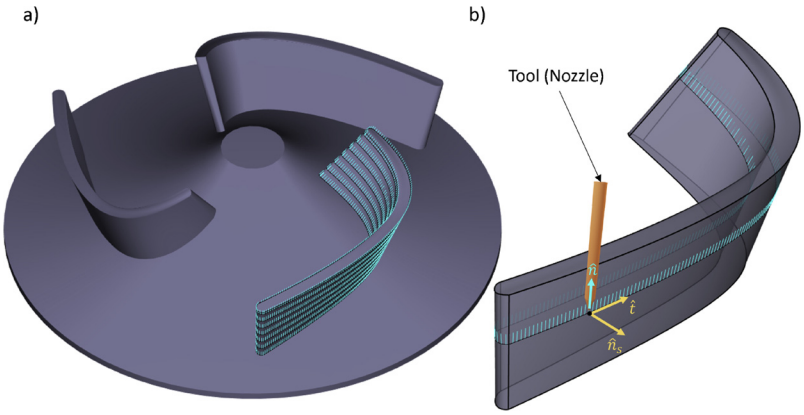

Fig. 7. Tool orientation along the 3D path applied in manufacturing of impeller blades.

mapped to connect the found points for each side surface at all the N layers. A mapped parametric line from point $p_1(u_1, v_1)$ to $p_2(u_2, v_2)$ on an arbitrary side surface $\boldsymbol{S}(u, v)$ demonstrated in Fig. 6, will result in a curve $\boldsymbol{C}(t)$ defined by Eq. 2 for $0 \leq t \leq 1$. Although these curves may differ a bit from the surface isoparametric curves, they provide the desired transition from the base to the top edges in the build direction.

$$\boldsymbol{C}(t) = \boldsymbol{S}(u_1 + (u_2 - u_1)t\,,\ v_1 + (v_2 - v_1)t) \tag{2}$$

The tool orientation is determined by the combination of SST orientation and the curved path directions found. The ideal orientation of the nozzle along a curve is perpendicular to the local curve tangent $\hat{t}$. Similarly, the SST condition constrains the orientation to be perpendicular to the local surface normal $\hat{n}_s$. With the constraints, illustrated in Fig. 7b, the tool orientation can be expressed by Eq. 3. Fig. 7 also points to an application of the path on an impeller blade side-surfaces where the hub and blade regions can be exclusively fabricated.

$$\hat{\boldsymbol{n}} = \frac{\hat{\boldsymbol{n}}_{\boldsymbol{s}} \times \hat{\boldsymbol{t}}}{|\hat{\boldsymbol{n}}_{\boldsymbol{s}} \times \hat{\boldsymbol{t}}|} \tag{3}$$

The use of the elaborated curve path and orientation is expected to result in no staircase effect on neither the side surfaces nor the top wall of the blade. An additional merit of the new path strategy is reduced retractions and non-extrusion passes which results in cleaner surfaces. Fig. 8 compares the fabrication methods of the impeller model shown Fig. 7a. Fig. 8a shows the impeller that is manufactured using path generated by a planar slicer on an STL version of the model with the aid of Simply3D software. The other impeller, shown in Fig. 8b, is created by initially manufacturing the hub using normal planar path g-codes. Afterwards, by appending the derived freeform path commands to the hub's g-codes, the impeller blades are fabricated.

The impeller fabrication process using planar slicer did not consider the form of the part manufactured. Hence, the occurrence of multiple islands and non-extrusion path could not be mitigated. The retraction and reloading of filament, made necessary by existence of islands, affect the surface quality of the part. The multi-axis path used allows tailoring of path for individual component in the model thereby ensuring good surface quality with minimal non-extrusion passes.

3.3. Toolpath for infill

The toolpath path for manufacturing the thin exterior surfaces of a given freeform part is studied in the previous section. However, as most models are required to be enclosed solids in applications, a method of fabricating the interior filled portion of a model is paramount to AM. Usually, due to high production time and the nature of FDM, solid model is hardly produced void-free. As a result, taking advantage of the ability to tailor infill density, use of completely gapless toolpath is rare. Rather, solids are usually manufactured using topological infill patterns that are easily filled after the outline of each layer is found. A common continuous pattern that can be easily generated is the zigzag pattern [31]. This filling pattern, commonly designed for planar toolpath, can be extended to fill a freeform surface with 3D curves.

From the model representation defined in Section 3.1, the freeform surfaces are not manufactured accurately using the present toolpath

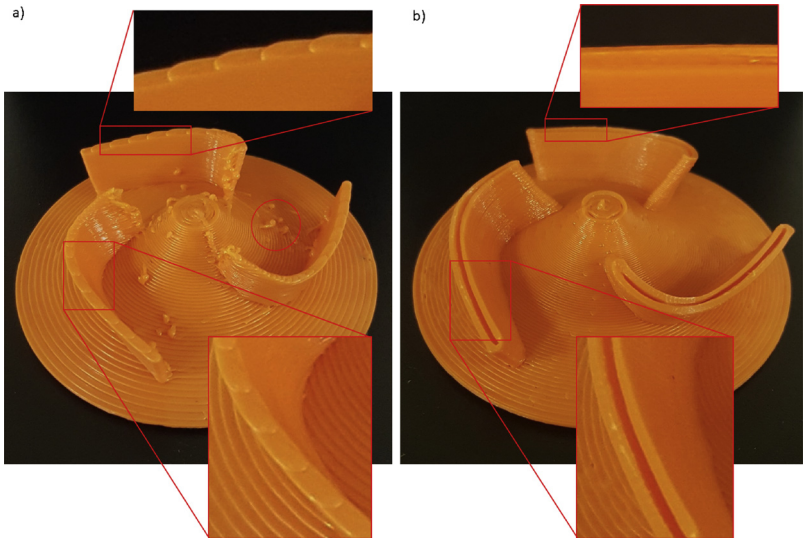

Fig. 8. Two impellers are manufactured, where a) traditional planar slicer is used, b) the blades are fabricated using the suggested path. Staircase effects are visible on the top wall of the impeller blades on the left. Retraction remnants are also visible on the hub and blade surfaces in a. The gaps in the blades of b can easily be filled using methods introduced in Section 3.3.

strategies in AM because of staircase effect. As mentioned in the previous section, SST tool orientation resolves this issue on the side surfaces. A method of filling the freeform model that results in staircase-free top surface is proposed in this section. Since the necessary tool orientation condition for a smooth top surface is the to keep the tool direction normal to the top surface, the proposed TSN orientation chooses the final deposition layer to coincide with the top surface. Furthermore, the infill layers can be designed in a way that they take the form of the top surface as they approach the final layer from the base surface. In other words, for n less than a total of layers N, a layer surface $\boldsymbol{L}(u, v)$ is such that $\boldsymbol{L}(u, v) = \boldsymbol{B}(u, v)$ and $\boldsymbol{L}(u, v) = \boldsymbol{T}(u, v)$ as $n \to 0$ and $n \to N$ respectively. To support compound models that can be expressed as combinations of multiple solid models of Section 3.1, material is deposited for the layers n = 1 up to n = N, since the base layer $\boldsymbol{B}(u, v)$ is assumed to be coincident with an existing base on a previously fabricated part without any gap. With the tool orientation on each layer maintaining the surface normal (TSN) condition, the top surface can be fabricated as the final layer without staircase effect. The transition layers should support the top layer while maintaining variable intra-layer thickness that do not exceed the maximum layer thickness, which is usually less than the nozzle diameter.

The concept of surface transition from one form to another is common in computer graphics [32], where it is usually referred as morphing. This study applies this notion to develop surfaces—as blends of the base and top surfaces—upon which infill paths are generated. The blending function is formulated as a mapping where one-to-one correspondence is established between the two surfaces. Fortunately, the organization of surfaces adopted in Section 3.1 ensures alignments of the (u, v) parameters of the two surfaces which can be matched to guarantee correspondence. Due to more even inter-layer thickness distribution along the build direction, a linear combination [33] or linear morph is chosen as the preferred blending function. The new surface representing nth layer is defined by Eq. 4.

$$\boldsymbol{L}(u, v) = \left(1 - \frac{n}{N}\right)\boldsymbol{B}(u, v) + \frac{n}{N}\boldsymbol{T}(u, v) \tag{4}$$

The transition layers do not take into consideration the shape of the side surfaces. Consequently, it is expected that the boundaries of the layers may not coincide with the side surfaces. In fact, the layer outline fits into boundary surfaces only when the side surfaces are obtained by lofting outline of the top surface linearly towards that of the base surface or vice versa. Fig. 9a demonstrates the possible mismatch where the blue surface boundaries lay outside the part's bounding surface(s) and the surface outline does not match the desired layer outline obtained by algorithm in Section 3.2. It should be noted that the shape of outline of the blue surface may deviated considerably from the orange outline in Fig. 9a, hence, mere translation cannot fix the issue. Evidently, as long as the mapping function does not take the boundary surfaces into consideration, the intermediate layers are bound to deviate from the model. It becomes pertinent to resolve this layer deviation issue to have a complete path planning scheme for a general freeform model.

Using methods outlined in Section 3.2, for each layer, the accurate outline can be extracted directly from the boundary surfaces. To get a proper surface, a new layer $\boldsymbol{L}'(u, v)$ is constructed by first designating the outline curves as its boundary. Hence, the curves $\boldsymbol{L}'(u, v_0)$, $\boldsymbol{L}'(u_1, v)$, $\boldsymbol{L}'(u, v_1)$ and $\boldsymbol{L}'(u, v_0)$ serve as the bounds of the surface $\boldsymbol{L}'(u, v)$. Where (u, v) are arbitrary parameters of the new surface with $u\varepsilon[u_0, u_1]$ and $v\varepsilon[v_0, v_1]$. Next, a method of transferring the shape of $\boldsymbol{L}(u, v)$ to the new surface $\boldsymbol{L}'(u, v)$ is proposed. With correspondence established between the two surfaces, a point on the surface $\boldsymbol{L}(u, v)$ on the u -directional isoparametric curve can be displaced by a vector $\boldsymbol{d^u}(u, v)$ interpolated between the determinable displacement vectors $\boldsymbol{L}'(u, v_0) - \boldsymbol{L}(u, v_0)$ and $\boldsymbol{L}'(u, v_1) - \boldsymbol{L}(u, v_1)$. The same point considered on the v -directional isoparametric curve will have an interpolated displacement vector given by $\boldsymbol{d^v}(u, v)$. The displacement vectors $\boldsymbol{d^u}(u, v)$ and $\boldsymbol{d^v}(u, v)$ are expressed in Eqs. 5 and 6 respectively.

$$\boldsymbol{d^u}(u, v) = \boldsymbol{L}'(u, v_0) - \boldsymbol{L}(u, v_0) + \frac{v - v_0}{v_1 - v_0}[\boldsymbol{L}'(u, v_1) - \boldsymbol{L}(u, v_1) - \boldsymbol{L}'(u, v_0) + \boldsymbol{L}(u, v_0)] \tag{5}$$

$$\boldsymbol{d^v}(u, v) = \boldsymbol{L}'(u_0, v) - \boldsymbol{L}(u_0, v) + \frac{u - u_0}{u_1 - u_0}[\boldsymbol{L}'(u_1, v) - \boldsymbol{L}(u_1, v) - \boldsymbol{L}'(u_0, v) + \boldsymbol{L}(u_0, v)] \tag{6}$$

It should be noted that the two displacements $\boldsymbol{d^u}(u, v)$ and $\boldsymbol{d^v}(u, v)$ are not equal. Since each carries some information on the shape of the new surface, a weighted average of the two is used to find the displacement given in Eq. 7. The overall displacement $\boldsymbol{d}(u, v)$, indicated in Fig. 9b, can be computed at any arbitrary (u, v) and can be used to create a proper transition layer.

$$\boldsymbol{d}(u, v) = \gamma\boldsymbol{d^u}(u, v) + (1 - \gamma)\boldsymbol{d^v}(u, v) \tag{7}$$

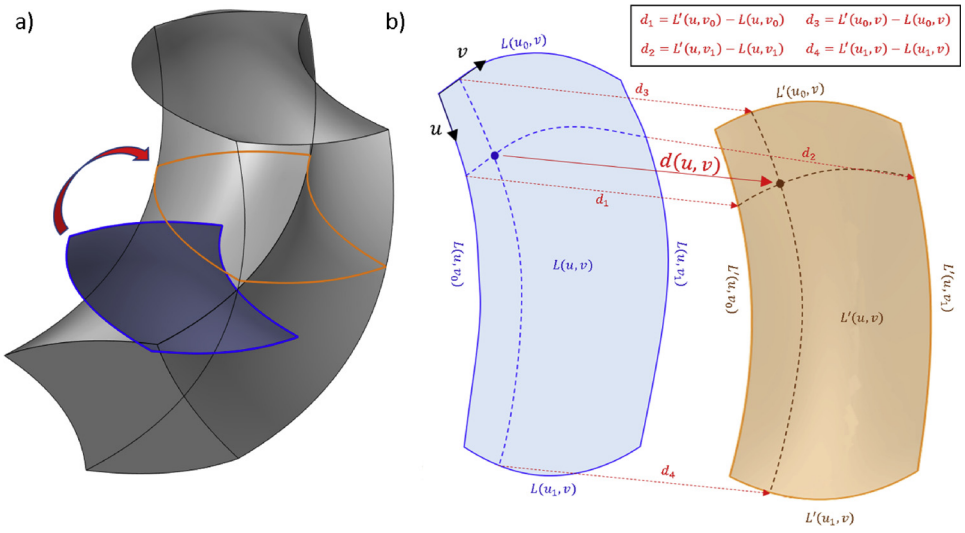

Fig. 9. a) The surface (in blue (u, v)) obtained by blending the top and base surfaces may not fit to the layer outline obtained using methods of Section 3.2. The shape of the blend surface needs to be transferred to the new layer $\boldsymbol{L}'(u, v)$ b) Construction of the new surface $\boldsymbol{L}'(u, v)$ by using combination of interpolated displacement vectors of the isoparametric curves of $\boldsymbol{L}(u, v)$ (For interpretation of the references to colour in this figure legend, the reader is referred to the web version of this article).

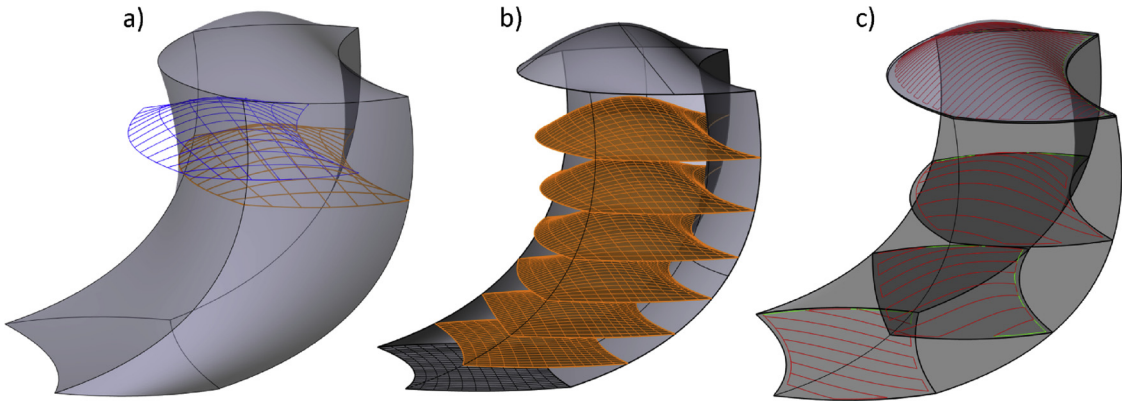

Fig. 10. For some layers from a model, an illustration of a) Networks curves(NCs) blended from $\boldsymbol{T}(u, v)$ and $\boldsymbol{B}(u, v)$ (blue) and the modified NCs (brown) that fit inside the model, b) some transition surfaces obtained from the NCs, c) zigzag path drawn on some surfaces (For interpretation of the references to colour in this figure legend, the reader is referred to the web version of this article).

Where γ and $(1-\gamma)$ represent the weights on the displacement vectors of the isoparametric u -curves and v -curves respectively. Upon adding the displacement vector to the blend surface, as expressed in Eq. 8, new transition surfaces can be explicitly obtained.

$$\begin{aligned}\boldsymbol{L}'(u,v) = \boldsymbol{L}(u,v) &+ \gamma\Big(\boldsymbol{L}'(u,v_0) - \boldsymbol{L}(u,v_0) \\ &+ \frac{v-v_0}{v_1-v_0}[\boldsymbol{L}'(u,v_1) - \boldsymbol{L}(u,v_1) - \boldsymbol{L}'(u,v_0) + \boldsymbol{L}(u,v_0)]\Big) \\ &+ (1-\gamma)\Big(\boldsymbol{L}'(u_0,v) - \boldsymbol{L}(u_0,v) + \frac{u-u_0}{u_1-u_0}[\boldsymbol{L}'(u_1,v) - \boldsymbol{L}(u_1,v) \\ &- \boldsymbol{L}'(u_0,v) + \boldsymbol{L}(u_0,v)]\Big)\end{aligned} \tag{8}$$

To construct the actual transition surfaces, network curves (NCs) are developed by mapping the isoparametric curves of $\boldsymbol{L}(u, v)$ to $\boldsymbol{L}'(u, v)$ using Eq. 8. Fig. 10a illustrates the resulting NCs in brown color. The designed plugin in this work generates all the AM layers using features that permit surface creation from NCs. The generated surfaces for some layers are shown in Fig. 10b. The general process of path generation of a closed freeform solid in the plugin is summarized in Fig. 11. Zigzag patterns are laid out for all layers in alternate directions on the rectangular parametric domain of the surfaces. After mapping those paths, 3D curve paths are obtained on the surfaces. Fig. 10c shows the 3D path on some layers, with the last couple of layers designed to have airtight hatch spacing.

A sample freeform part enclosed by completely non-planar surfaces is fabricated using the strategy discussed in this section. Fig. 12a shows the freeform model whose base surface is attached to an initial part that was fabricated by normal planer 3-axis path. For comparison, the model is fabricated as a traditional 3-axis FDM using the flat layers shown in Fig. 12b. The formulated 5-axis path, shown in Fig. 12d, is applied to the model from the base to the top layers using a material deposition that corresponds to the variable layer spacings demonstrated in the figure. The manufacturing instant shown in Fig. 12e reveals the infill pattern obtained by the generated layer paths. The same paths smaller hatch spacings are used in the final 3 layers to obtain the top surface. All the paths used, including the layer outlines paths, have tool direction defined by the TSN tool orientation. By comparing the objective of layering and infilling method, the top surfaces of the manufactured samples are compared in Fig. 12c and f.

For parts that can be expressed as compound models composed of the freeform model schemes introduced, the developed process plan can be adopted for such parts where the individual freeform model is fabricated in sequence. Fig. 13 shows a sample compound model where the 5-axis scheme is applied for the parts 2, 3 and 4. The sample layer paths, thickness distributions and tool directions are shown in the figure. The regions are fabricated in sequence part 1,2,3 and4, where the initial part is produced using planar layers.

For comparison, the 5-axis additive manufacturing of the sample compound model is also compared with the horizontal layer FDM in Fig. 14.Top surfaces are showcased with reduced breaks and

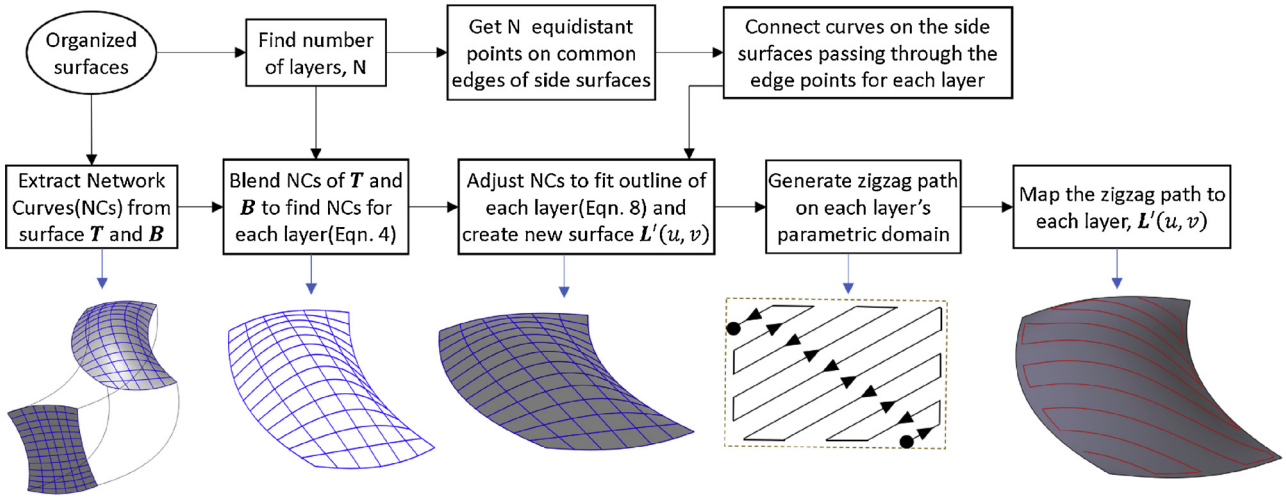

Fig. 11. Outline of stages of path planning from surfaces extracted from a CAD model.

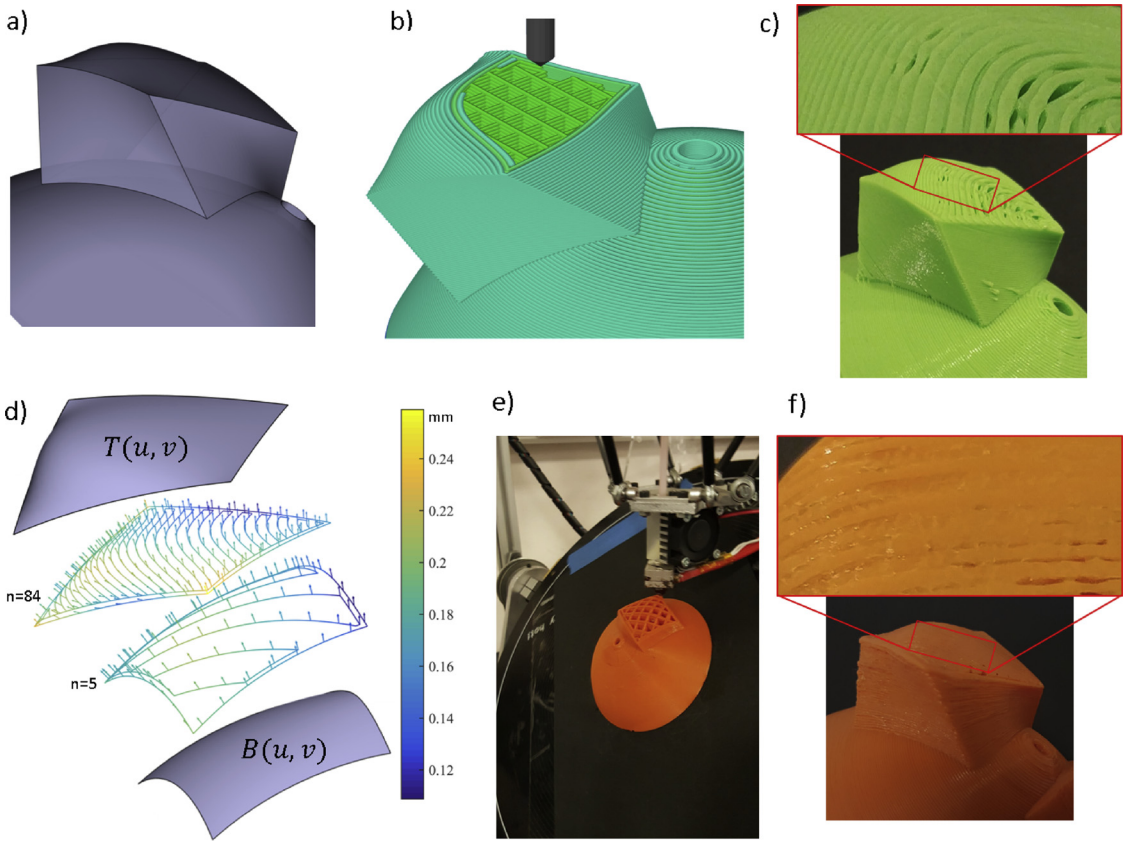

Fig. 12. a) A sample freeform CAD model to be manufactured. b) Horizontal layer paths used in manufacturing the model for comparison. c) The manufactured sample using plan in (b). d) The base, top(n = 85), 5th and 84th layers with the 5-axis paths showing the layer gap distribution on the color scale and the tool directions e) The fabrication instant using the designed 5-axis 3D printer showing the infill of the proposed paths of transition layers. f) The final manufactured part using plan in (e).

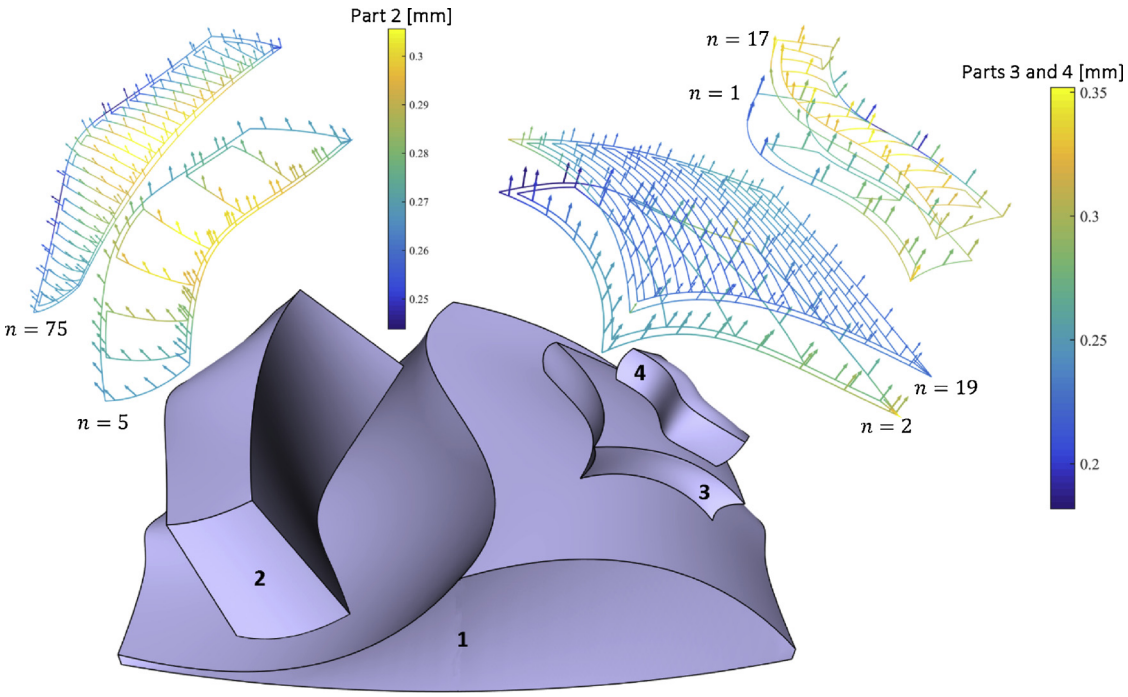

Fig. 13. A sample compound model composed of regional parts is tested using the 5-axis process plan to produce Sections 2,3, and 4. The parts 2, 3, 4 have total of 75, 21 and 17 layers respectively.

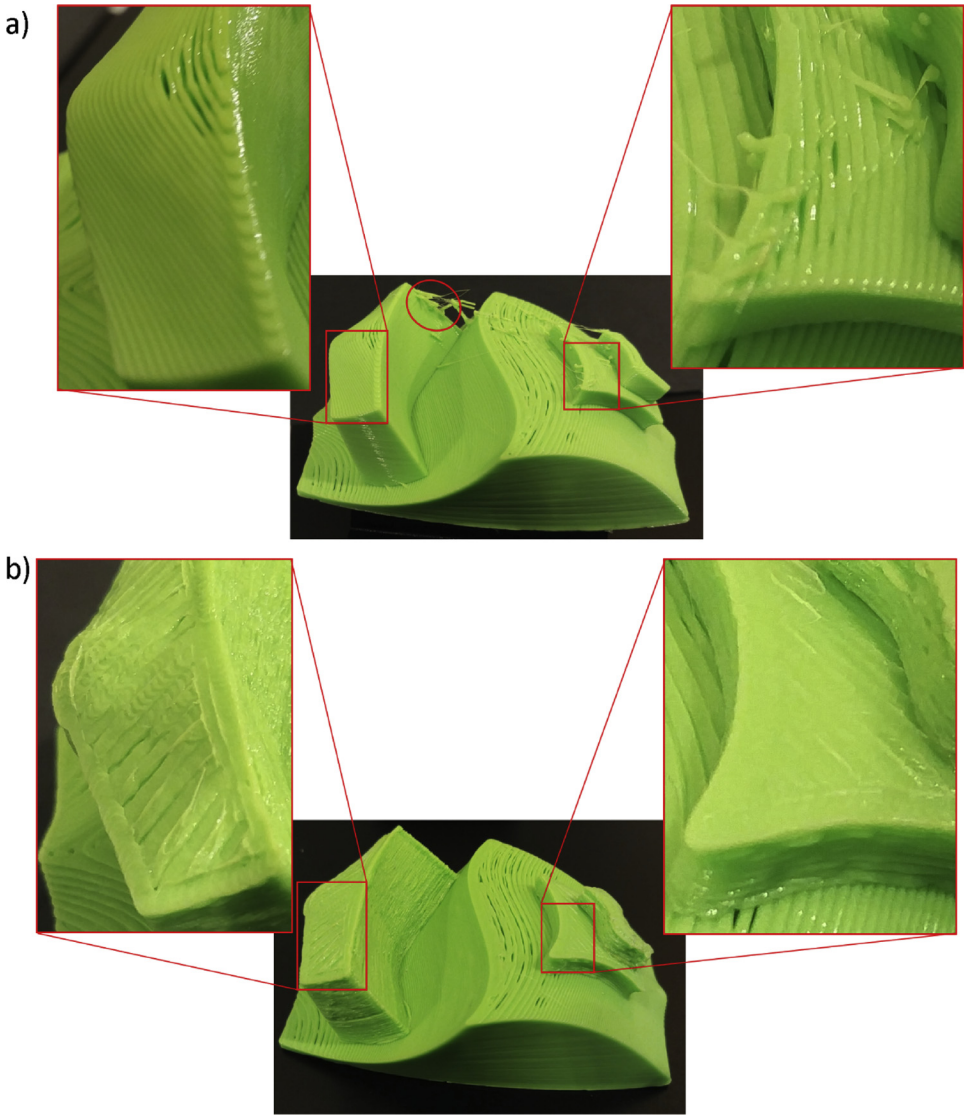

Fig. 14. a) The compound model in Fig. 13 is produced by horizontal layer FDM for comparison. b) The 5-axis AM method is used to fabricate parts 2, 3 and 4. Marked regions show the advantages of using the method in this paper.

unevenness in many regions. The added advantage of more efficient path with less non-extrusion motion shows reduced residual drops caused by tool retractions.

4. Evaluation of build angles and kinematic error

Generated toolpath for multi-axis AM comes with tool directions which represent the desired relative orientations of the tool with respect to the part. It is therefore required for either the tool or the part to transform to positions that correspond to the configurations. In the case of the built 5-axis 3D printer, a movable print-bed accomplishes the task of orientation.

For a desired build orientation given by the unit vector $\boldsymbol{n}_b = \langle n_x, n_y, n_z \rangle^T$ the corresponding angles $\phi \varepsilon \left[-\frac{\pi}{2}, \frac{\pi}{2}\right]$ and $\theta \varepsilon [-\pi, \pi]$ shown in Fig. 15a are found by transforming the print-bed from the default orientation facing Z-direction ($\langle 0,0,1 \rangle^T$) to $\boldsymbol{n_b}$. By evaluating the inverse kinematics of the platform transformation, $\boldsymbol{n_b} = \boldsymbol{R_z}(\theta) \cdot \boldsymbol{R_y}(\phi) \cdot \langle 0,0,1 \rangle^T$, Eq. 9 is obtained. Equating Eq. 9 with the components of $\boldsymbol{n_b}$ leads to the expressions in Eqs. 10 and 11. The angle θ has two solutions $\theta_1 = atan2(n_y, n_x)$ and $\theta_2 = atan2(-n_y, -n_x)$ for which ϕ is positive and negative respectively. Considering a preceding angle θ_{i-1}, there are four possible paths from θ_{i-1} to θ as indicated Fig. 15b. Among the four possibilities, there is always the shortest path where the change, $|\Delta\theta| \leq \frac{\pi}{2}$. The decision on the next value of θ is made using Eqs. 10 and 11, where the value of σ is found by Eq. 12. The firmware is programmed to make the decision on which direction of rotation is shorter.

$$\boldsymbol{n_b} = \begin{bmatrix} -\cos(\theta)\sin(\phi) \\ -\sin(\theta)\sin(\phi) \\ \cos(\phi) \end{bmatrix} \tag{9}$$

$$\theta = atan2(\sigma n_y, \sigma n_x) \text{ (For the case } n_x \neq 0 \text{ or } n_y \neq 0) \tag{10}$$

$$\phi = \text{atan}\left(\frac{\sigma\sqrt{n_x^2 + n_y^2}}{n_z}\right) \tag{11}$$

Where the value of σ is given by Eq. 12.

$$\sigma = \begin{cases} 1 \; if \; |\theta_1 - \theta_{i-1}| \leq \frac{\pi}{2} \; or \; 2\pi - |\theta_1 - \theta_{i-1}| < \frac{\pi}{2} \\ -1 \; if \; |\theta_2 - \theta_{i-1}| \leq \frac{\pi}{2} \; or \; 2\pi - |\theta_2 - \theta_{i-1}| < \frac{\pi}{2} \end{cases} \tag{12}$$

A critical point in 5-axis inverse kinematics is when $n_x = 0$ and $n_y = 0$. Theoretically, Eq. 9 does not have a solution for θ at this

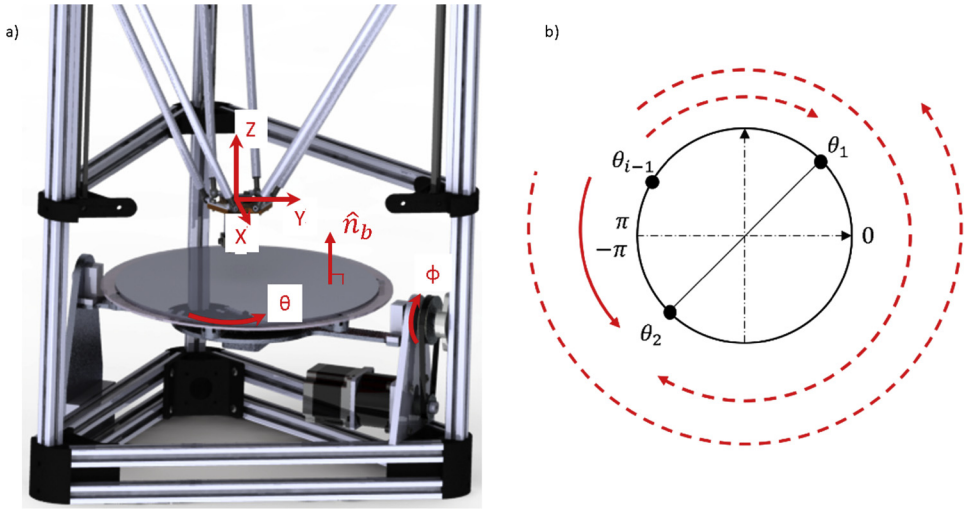

Fig. 15. a) Print-bed that can be oriented to a desired build direction. b) The four possible paths of θ solution.

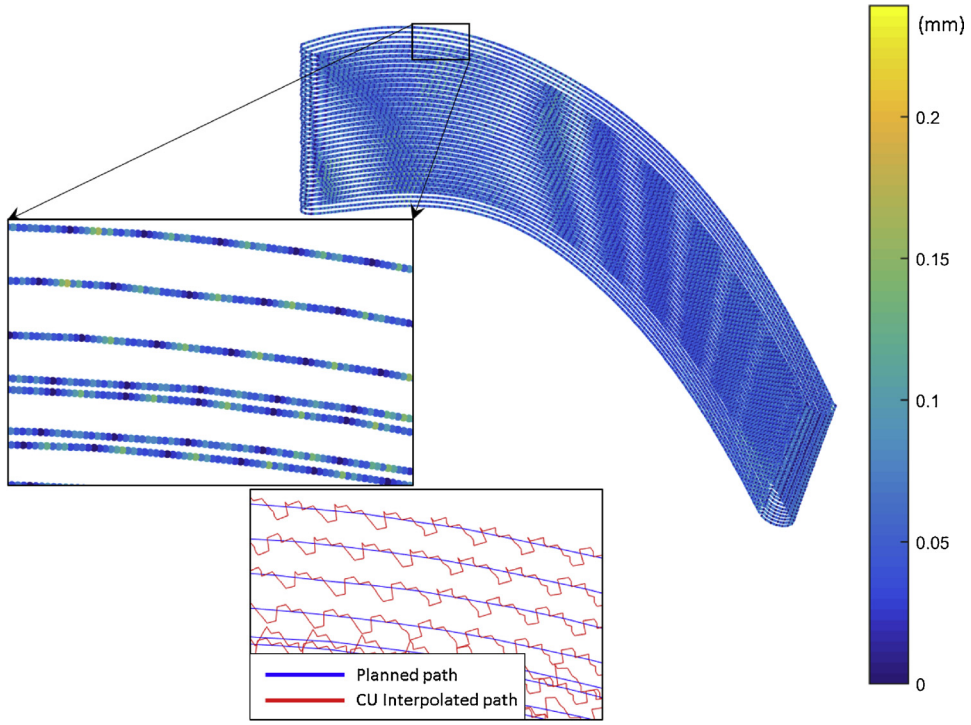

Fig. 16. Distribution of kinematic error and plot of interpolator trajectory along the deposition path of the impeller blade fabricated in Fig. 9.

location, and axis C does not have any influence on the orientation of the print-bed. Practically, near this point, dangerously abrupt motion of axis C can occur. This complication is ascribed to the interpolation carried out in the numerical control units in joint space of the base platform. Within the interpolation spectrum, the singularity can be traversed and large non-linear deviation from the planned path can be observed. The large deviation is caused by the fact that the change in consecutive θ values can be large even when the change in $\boldsymbol{n_b}$ is very small. As a remedy, Affouard et al. [34] adopted the concept of singularity cone to account for the uncertainties in the angle ϕ. It provides a range close to the singular point where the solution using Eq. 9 can lead the tool to traverse the singularity point. Whenever a path points are detected within the singularity cone, the values of angle θ are obtained by patching between two points, one before entering the cone, the other after exiting it. Decision on how far the points must be from the cone is made based on the path length and change of angle θ between the two points. The method used in this article is the combination of the singularity cone idea [34] with a C-axis patching strategy [35] proposed by Grandguillaume et al.

It is important to point out that interpolation on the transformed position implemented in the firmware generates kinematic error at all interpolation steps within a line segment. The presence of angular positions makes the error different from mere linearization error. Although, the error increases when the configuration of the bed is close to singularity. It becomes crucial to estimate the magnitude of these errors for every path g-code before the commands are sent to the 3D printer. Kinematic errors are computed using the method outlined by Makhanov et al. [36]. The errors are obtained through evaluation of the difference between re-transformed path (from printer to workpiece frame) of interpolated g-code points with the original desired path. The estimated result of the kinematic error of the impeller blade path is shown in Fig. 16. During path planning, the path is sampled at curve

length of 0.6 mm while the interpolation resolutions of 0.1 mm for each of XYZ positions, 0.02 mm for filament extrusion, 0.06° for B axis and 0.1° for C axis are used. It should be noted that decreasing these resolutions will not improve the kinematic error and decreasing the sampling curve length will lead to increase in manufacturing time and large size of g-code files. The estimated error plot is used for g-code inspection before 3D printing.

5. Discussion and conclusion

Using a designed and built 5-axis additive manufacturing system, process and path planning techniques are studied for arbitrary shell and solid freeform components. Software script that performs the functions of both toolpath generation and postprocessing are programmed. By connecting mapped parametric lines on the side NURBS surfaces of a solid part, 3D curves that transition from the base to the top profile of the wall are obtained. Using these curves along with side surface tangent tool orientation, shell parts are shown to be fabricated without staircase effects. The idea of transition layering from base to top surface of a solid freeform part is introduced. AM paths are planned on the constructed surfaces with surface-normal tool orientation to prevent staircase effects on the top portion of the freeform solid parts.

Even with the presence of kinematic errors, the benefits of using the stipulated path planning strategies are apparent on test specimens. For the freeform filled sample fabricated in this paper, the ideal tool orientation along the outline of each layer should be obtained by the SST rule indicated in Section 3.2. This orientation is not used because of the requirement for numerous fast retractions that cannot be realized on the 3D printer. When the retracted nozzle in a layer is not repositioned quick enough, the filament material oozes out, thereby affecting surface quality of subsequent layers. This is caused by limitations on speed of the control system and motors.

This paper explores new methods of 5-axis additive manufacturing of freeform models to maintain surface quality and provide efficient toolpaths. Improvements are still required in actuation, control system, and reduction of kinematic errors.

Competing interests

None

Acknowledgement

This research was supported by the Koc University, Manufacturing and Automation Research Center, Istanbul, Turkey.

References

[1] Gao W, Zhang Y, Ramanujan D, Ramani K, Chen Y, Williams CB, et al. The status, challenges, and future of additive manufacturing in engineering. CAD Comput Aided Des 2015;69:65–89. https://doi.org/10.1016/j.cad.2015.04.001.
[2] Matsuzaki R, Ueda M, Namiki M, Jeong T-K, Asahara H, Horiguchi K, et al. Three-dimensional printing of continuous-fiber composites by in-nozzle impregnation. Sci Rep 2016;6:23058. https://doi.org/10.1038/srep23058.
[3] Huang Y, Leu MC, Mazumder J, Donmez A. Additive manufacturing: current state, future potential, gaps and needs, and recommendations. J Manuf Sci Eng 2015;137:014001https://doi.org/10.1115/1.4028725.
[4] Wulle F, Coupek D, Schäffner F, Verl A, Oberhofer F, Maier T. Workpiece and machine design in additive manufacturing for multi-axis fused deposition modeling. Procedia CIRP 2017;60:229–34. https://doi.org/10.1016/j.procir.2017.01.046.
[5] Chen JSS, Feng HY. Optimal layer setup generation in layered manufacturing with a given error constraint. J Manuf Syst 2011;30:165–74. https://doi.org/10.1016/j.jmsy.2011.07.001.
[6] Jin YA, Li H, He Y, Fu JZ. Quantitative analysis of surface profile in fused deposition modelling. Addit Manuf 2015;8:142–8. https://doi.org/10.1016/j.addma.2015.10.001.
[7] Chakraborty D, Aneesh Reddy B, Roy Choudhury A. Extruder path generation for curved layer fused deposition modeling. CAD Comput Aided Des 2008;40:235–43. https://doi.org/10.1016/j.cad.2007.10.014.
[8] Llewellyn-Jones T, Allen R, Trask R. Curved layer fused filament fabrication using automated toolpath generation. 3D Print Addit Manuf 2016;3:236–43. https://doi.org/10.1089/3dp.2016.0033.
[9] Allen RJA, Trask RS. An experimental demonstration of effective Curved Layer Fused Filament Fabrication utilising a parallel deposition robot. Addit Manuf 2015;8:78–87. https://doi.org/10.1016/j.addma.2015.09.001.
[10] Jin Y, Du J, He Y, Fu G. Modeling and process planning for curved layer fused deposition. Int J Adv Manuf Technol 2017;91:273–85. https://doi.org/10.1007/s00170-016-9743-5.
[11] Ahn S, Montero M, Odell D, Roundy S, Wright PK. Anisotropic material properties of fused deposition modeling ABS. Rapid Prototyp J 2002;8:248–57. https://doi.org/10.1108/13552540210441166.
[12] Singamneni S, Roychoudhury A, Diegel O, Huang B. Modeling and evaluation of curved layer fused deposition. J Mater Process Technol 2012;212:27–35. https://doi.org/10.1016/j.jmatprotec.2011.08.001.
[13] Castelino K, D'Souza R, Wright PK. Toolpath optimization for minimizing airtime during machining. J Manuf Syst 2003;22:173–80. https://doi.org/10.1016/S0278-6125(03)90018-5.
[14] Guo Q, Sun Y, Jiang Y, Yan Y, Zhao B, Ming P. Tool path optimization for five-axis flank milling with cutter runout effect using the theory of envelope surface based on CL data for general tools. J Manuf Syst 2016;38:87–97. https://doi.org/10.1016/j.jmsy.2015.11.003.
[15] Shen H, Huiadong D, Shuhua Y, Fu J. Fused deposition modeling 5-axis additive manufacturing: machine design, fundamental printing methods and critical process characteristics. Rapid Prototyp J 2017. https://doi.org/10.1108/RSR/-10-2016-0070.
[16] Lee K, Jee H. Slicing algorithms for multi-axis 3-D metal printing of overhangs. J Mech Sci Technol 2015;29:5139–44. https://doi.org/10.1007/s12206-015-1113-y.
[17] Kallevik G. 5-axis 3D Printer-Designing a 5-axis 3D printer. University of Oslo; 2015.
[18] Keating S, Oxman N. Compound fabrication: a multi-functional robotic platform for digital design and fabrication. Robot Comput Integr Manuf 2013;29:439–48. https://doi.org/10.1016/j.rcim.2013.05.001.
[19] Le VT Paris H, Mandil G. Process planning for combined additive and subtractive manufacturing technologies in a remanufacturing context. J Manuf Syst 2017;44:243–54. https://doi.org/10.1016/j.jmsy.2017.06.003.
[20] Jones R, Haufe P, Sells E, Iravani P, Olliver V, Palmer C, et al. Reprap - the replicating rapid prototyper. Robotica 2011;29:177–91. https://doi.org/10.1017/S026357471000069X.
[21] Graves S, Rocholl J, Marlin H, Clear K, Labs BE, Rostock T, et al. Rocholl (Rostock) style Delta robot kinematics. 2012.
[22] Song X, Pan Y, Chen Y. Development of a low-cost parallel kinematic machine for multidirectional additive manufacturing. J Manuf Sci Eng 2015;137:021005https://doi.org/10.1115/1.4028897.
[23] Yerazunis WS, Barnwell JCI, Nikovski DN. Strengthening ABS, nylon, and polyester 3D printed parts by stress tensor aligned deposition paths and five-axis printing. Solid Free Fabr Symp 2016:1259–71. https://doi.org/10.1021/acsnano.6b02108.
[24] Scott L, Neufeld R, Bob K, Erik Z. Marlin 3D printer firmware. Github repos. 2017 (Accessed 23 December 2016). https://github.com/MarlinFirmware/Marlin.
[25] Mani K, Kulkarni P, Dutta D. Region-based adaptive slicing. CAD Comput Aided Des 1999;31:317–33. https://doi.org/10.1016/S0010-4485(99)00033-0.
[26] ming Zhao H, He Y, J zhong Fu, jiang Qiu J. Inclined layer printing for fused deposition modeling without assisted supporting structure. Robot Comput Integr Manuf 2018;51:1–13. https://doi.org/10.1016/j.rcim.2017.11.011.
[27] Willem FB, Frederik WJ, Frits HP. Design and display of solid models. Adv. Comput. Graph. VI-Images Synth. Anal. Interaaction 2005:1–57. https://doi.org/10.1016/B978-0-12-227741-2.50028-1.
[28] Piegl L, Tiller W. The NURBS book. 2nd ed. Springer; 1997. https://doi.org/10.1007/978-3-642-59223-2.
[29] Jin GQ, Li WD, Tsai CF, Wang L. Adaptive tool-path generation of rapid prototyping for complex product models. J Manuf Syst 2011;30:154–64. https://doi.org/10.1016/j.jmsy.2011.05.007.
[30] Zhao G, Ma G, Feng J, Xiao W. Nonplanar slicing and path generation methods for robotic additive manufacturing. Int J Adv Manuf Technol 2018:1–11. https://doi.org/10.1007/s00170-018-1772-9.
[31] an Jin Y, He Y, J zhong Fu, feng Gan W, wei Lin Z. Optimization of tool-path generation for material extrusion-based additive manufacturing technology. Addit Manuf 2014;1:32–47. https://doi.org/10.1016/j.addma.2014.08.004.
[32] Ju T, Goldman R. Morphing rational B-spline curves and surfaces using mass distributions. Eurographics 2003:0–7.
[33] Piegl L, Tiller W. Symbolic operators for NURBS. CAD Comput Aided Des 1997;29:361–8. https://doi.org/10.1016/S0010-4485(96)00074-7.
[34] Affouard A, Duc E, Lartigue C, Langeron JM, Bourdet P. Avoiding 5-axis singularities using tool path deformation. Int J Mach Tools Manuf 2004;44:415–25. https://doi.org/10.1016/j.ijmachtools.2003.10.008.
[35] Grandguillaume L, Lavernhe S, Tournier C. A tool path patching strategy around singular point in 5-axis ball-end milling. Int J Prod Res 2016;54:7480–90. https://doi.org/10.1080/00207543.2016.1196835.
[36] Makhanov SS, Anotaipaiboon W. Advanced numerical methods to optimize cutting operations of five-axis milling machines. 2007. https://doi.org/10.1007/978-3-540-71121-6.